

PAPER • OPEN ACCESS

## FTIR spectroscopy characterization and critical comparison of poly(vinyl)alcohol and natural hydroxyapatite derived from fish bone composite for bone-scaffold

To cite this article: May Teng Hooi *et al* 2021 *J. Phys.: Conf. Ser.* **2120** 012004

View the [article online](#) for updates and enhancements.

You may also like

- [Fabrication and Characterisation of Gelatine/Hydroxyapatite Porous Scaffold](#)  
M.I. Mazlam, H.H. Ho and A. Nurazreena
- [Fibronectin adsorption on osteoconductive hydroxyapatite and non-osteoconductive - alumina](#)  
Maki Hasegawa, Tada-aki Kudo, Hiroyasu Kanetaka et al.
- [Comparison of \*in vitro\* and \*in vivo\* bioactivity: cuttlefish-bone-derived hydroxyapatite and synthetic hydroxyapatite granules as a bone graft substitute](#)  
Beom-Su Kim, Hyo Jin Kang, Sun-Sik Yang et al.



The Electrochemical Society  
Advancing solid state & electrochemical science & technology

### 241st ECS Meeting

May 29 – June 2, 2022 Vancouver • BC • Canada

Extended abstract submission deadline: Dec 17, 2021

Connect. Engage. Champion. Empower. Accelerate.  
**Move science forward**



**Submit your abstract**



# FTIR spectroscopy characterization and critical comparison of poly(vinyl)alcohol and natural hydroxyapatite derived from fish bone composite for bone-scaffold

May Teng Hooi, Siew Wei Phang\*, Hui Ying Yow, Edmund David, Ning Xin Kim, Hui Leng Choo

School of Computer Science and Engineering, Taylor's University Malaysia, 1, Jalan Taylors, 47500 Subang Jaya, Selangor, Malaysia

\*Corresponding author: [eunicepsw@gmail.com](mailto:eunicepsw@gmail.com)

**Abstract.** This paper presents the interaction comparison of poly(vinyl) alcohol (PVA) with hydroxyapatite derived from Spanish Mackerel (SM) and Whitefin Wolf Herring (WWH) bones, in different processing method. PVA filament and solution casting method illustrated higher crystallinity in the FTIR graph as compared to the PVA pellet and filament extrusion method. Besides, minimal interactions between PVA with glycerol and HAp was observed as well. PVA pellet and solution casting method portrait higher interaction as compared to the PVA filament and extrusion method. As for the HAp of SM and WWH, WWH had higher crystallinity and better cell adhesion with a higher Ca/P ratio while SM had relatively better mechanical strength with Ca/P ratio near to stoichiometric value. The loading of HAp (0, 2.5, 5, 10, 20, 30%) does not affect interactions of PVA/HAp composite in FTIR, and thermal properties in TGA. However, it caused an increase in crystallinity at low HAp loading and decreased at higher loading of HAp above 10%. Upon addition of HAp, tensile strength increased and elongation at break decreased. As the loading of HAp increased, both mechanical properties decreased. Scaffold with WWH composite possessed lower tensile strength and higher elongation at break than SM composite. The result of mechanical properties corresponded to the SEM result. ANOVA analysis justified the effect of HAp variations and loading on the mechanical properties of the composite was prominent.

## 1. Introduction

Bone healing process is complicated as it is affected by numerous factors such as defect size, location, cellular response, and more [1]. The field of Tissue Engineering was introduced to restore, maintain, or improve the tissue functions and simplify the bone healing process [2]. In the context of Bone Tissue Engineering (BTE) a scaffold is a common approach as it is a bioactive material that can prevent any adaptive issues while promoting bone healing [3]. Different wound application requires different features and performance of bone scaffold.

Bio-composites composed of hydroxyapatite (HAp) and poly (vinyl alcohol) (PVA) have been widely studied and developed for BTE [4]. Scaffold with PVA/HAp has good bioactivity and mechanical properties [5]. Fish bones are one of the natural sources for the extraction of HAp with rich calcium and phosphate element [6]. The bones of Spanish Mackerel (SM) and Whitefin Wolf Herring (WWH) were used to extract HAp because they are widely accessible and have no conflict in religious means [7]. Different sources of HAp have different properties such as porosity, crystallinity, and composition that would affect its application. PVA is widely used in the medical field as it is FDA approved for medical use and low cost with good mechanical strength [8]. There is a variety of PVA in terms of their variation,



Content from this work may be used under the terms of the [Creative Commons Attribution 3.0 licence](https://creativecommons.org/licenses/by/3.0/). Any further distribution of this work must maintain attribution to the author(s) and the title of the work, journal citation and DOI.

forms, degree of hydrolysis, molecular weight, etc. Generally, PVA has common difficulties in thermal processing [9]. Modification such as adding glycerol as a plasticizer can alter the hydrogen bonding of PVA and lower its melting point to enhance its thermal processability [10].

In terms of the fabrication method of the bone scaffold, there are two main categories which are the conventional method and the rapid prototyping method. In this paper, the solution casting as conventional technique and filament extrusion for Fused Deposition Modeling (FDM) as a rapid prototyping technique was applied. The material used for different fabrication methods required to possess suitable properties that suit the nature of the fabrication method. The characterization of the scaffold is important to justify if the material used for the bone scaffold is suitable for the application of BTE.

Vibrational spectroscopy allows the study and analysis of the morphological aspect of the material to understand the physical properties such as crystallinity, mechanical response, or failure condition. The synergistic effect and binding mechanisms of composite material can be investigated as well [11,12]. In the present work, FTIR spectroscopy analysis was performed to study the variation of PVA in pellet and filament form with respective plasticizing effects with glycerol, the composite interaction with different scaffold fabrication methods of solution casting and filament extrusion, and the differences in natural HAp derived from different fish bones. Furthermore, the scaffold fabricated with different loading and sources of natural HAp was characterized to study the effect of these factors on the scaffold properties. The interaction between composite and the understanding of material network structure provides crucial information to the development of tissue engineering scaffolds with properties that can fulfill stringent requirements and applications.

## 2. Material and Methods

### 2.1. Material

The fish bones of *Scomberomorus commerson*, known as Spanish Mackerel (SM) or “Ikan tenggiri” in Malay language and *Chirocentrus nudus*, known as Whitefin Wolf Herring (WWH) or “Ikan parang”, were obtained from local fish stalls in Kuala Lumpur, Malaysia. The bones were stored in the freezer for preservation. Poly(vinyl) alcohol (PVA) with 88.3% partial hydrolysis was purchased from R&M Chemical. Glycerol with 99.5% purity was obtained from Merck Sdn. Bhd., Malaysia. PVA filament was purchased from Ultimaker. All materials were used as received.

### 2.2. Preparation of Hydroxyapatite and Plasticization of Poly(Vinyl) Alcohol

The fish bones cleaning and calcination process were as mentioned by the authors [7]. Briefly, the spine parts were selected and boiled in water for 1 hour followed by cleaning to remove organic components. The bones were dried in oven at 80°C overnight, then calcinated in the furnace at 800°C for 4 hours with a heating rate of 10°C/min. After cooling, the bones were grinded to powder and sieved with a mesh size of 150 µm.

Plasticization of PVA involved homogenous mixing 100 phr of PVA, 20 phr of glycerol, and 20 phr of distilled water. The blend was placed in a sealed beaker at 40 °C for 8 hours.

### 2.3. Scaffold Fabrication with Solution Casting and Filament Extrusion

Two batches of solution cast film were fabricated, one with SM HAp composite and the other with WWH HAp composite. Solution casting began with 10 g PVA pellet mixed with 100 mL water and 2 mL glycerol in a hot water bath maintained at  $97 \pm 3$  °C for 1 hour. The solution was constantly stirred at 500 rpm with a mechanical stirrer to avoid agglomeration of powder. The measured amount of HAp powder from both fishes was added to the solution according to the composition listed in Table 1. The solution was then homogenized under 16000 rpm for 10 minutes to evenly disperse the HAp in the

solution. The homogenized solution was poured into 135 mm petri dish with controlled thickness at 2mm. The dish was placed in a 60 °C oven for overnight drying.

Filament extrusion began with 5 phr SM HAp added and homogeneously mixed with 100 phr plasticized PVA filament. The mixture was fed into with Wellzoom Desktop Extruder Line II single screw extruder with a screw speed of 10. The screw temperature was set at 180 °C and the nozzle temperature was set at 185°C. The diameter of the filament was adjusted to be 1.75 ±0.05 mm.

**Table 1.** Composition of HAp/PVA composite for solution casting

Samples	PVA as Base Polymer (phr)	Distilled Water (phr)	Glycerol (phr)	HAp (phr)	
				SM	WWH
Pure PVA	100	1000	20	0	0
2.5HAp/PVA	100	1000	20	2.5	2.5
5.0HAp/PVA	100	1000	20	5.0	5.0
10HAp/PVA	100	1000	20	10	10
20HAp/PVA	100	1000	20	20	20
30HAp/PVA	100	1000	20	30	30

#### 2.4. Scaffold sample characterisation

Fourier transform infrared spectrometer (FTIR) enabled the study of chemical composition and variation in the molecular structure. FTIR was operated at a range of 400 to 4,000  $\text{cm}^{-1}$  with resolution of 4  $\text{cm}^{-1}$ . The samples for FTIR testing were the pure and plasticized PVA pellet and filament, glycerol, solution casted film with 5HAp/PVA, extruded filament with 5HAp/PVA, SM HAp, WWH HAp, and all solution cast film with SM and WWH composite at 0, 2.5, 5, 10, 20, and 30% HAp loading.

The following characterization tests were implemented on all solution cast film with SM and WWH composite at 0, 2.5, 5, 10, 20, and 30% HAp loading. Energy-dispersive X-ray spectroscopy (EDX) was used to determine the composition of calcium to phosphate (Ca/P) ratio in the scaffold. The EDX equipment displayed composition in wt%. Scanning electron microscopy (SEM) used to understand the morphology condition of the material. It was performed at 1 kV and 20 kV to generate micrographs for visual analysis [13]. Thermogravimetric analysis (TGA) enabled the study of the thermal behavior of composite. Under nitrogen flow, 5mg of each sample was heated from 30 °C to 750 °C at a heating rate of 20 °C/min. For mechanical property analysis, each sample was prepared in 6 mm wide and 8 cm long rectangular strips. Tensile strength signifies resistance of scaffold to break under tension or elongation. The samples were clamped with 5 cm distance and tested according to the ASTM D882 standard. A constant tensile deformation of 25 mm/min was applied until fracture occurred. Each sample was performed with 5 repetitions for accurate data. The data from tensile testing was used to perform Analysis of Variance (ANOVA) 2 ways with Microsoft Excel.

### 3. Results and discussion

#### 3.1. Interaction between variations in poly(vinyl) alcohol

In this study, the vibrational spectroscopy of the variation of poly(vinyl) alcohol (PVA), in the form of pellet and filament were investigated. The properties of PVA affects its application in the field of bone tissue engineering, for example in the various scaffold fabrication method of a bone scaffold.

By analyzing the FTIR curve of variations in PVA in Fig. 1, both PVA had nearly identical curves that suggested they had similar functional groups and properties of PVA. The large predominant band at  $3100\text{ cm}^{-1}$  to  $3600\text{ cm}^{-1}$  attributed to hydroxyl  $OH$  groups [14]. The duplet peaks between  $2900\text{ cm}^{-1}$  to  $3000\text{ cm}^{-1}$  associated to  $CH_2$  group, whereby the peak at higher wavenumber represent asymmetric and the lower wavenumber represent symmetric stretching of  $CH_2$  group [15]. The peak at  $1710\text{ cm}^{-1}$  attributed to  $C=O$  and  $C-O$  of acetate group [16]. Information regarding crystallinity of PVA was given by the peak at  $1140\text{ cm}^{-1}$  associated to  $C-O-C$  stretching [17].

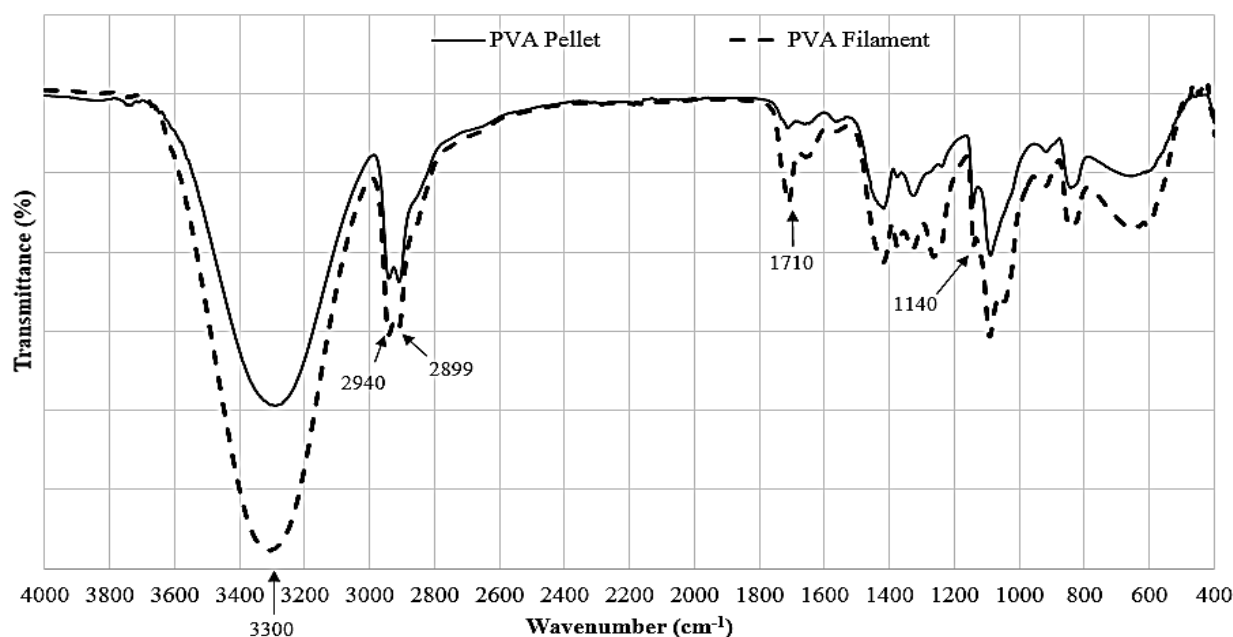


**Figure 1.** FTIR Graph of PVA pellet and PVA filament

PVA filament had been commercially processed so it had slightly different properties than conventional PVA pellets. PVA filament possessed a higher degree of crystallinity as compared to PVA pellet with taller peak intensity at  $1140\text{ cm}^{-1}$ . The crystallinity and molecular entanglements are dependent on the hydrophilic/hydrophobic force balance where hydrogen bonds are responsible for hydrophilic associated properties [18]. This was further supported by many hydroxyl groups present in PVA filament with higher band intensity at  $3300\text{ cm}^{-1}$ . PVA filament had complex molecular structure. The peak at  $2940\text{ cm}^{-1}$  representing asymmetric  $CH_2$  group had faster energy transfer due to shorter distance to its abundant neighboring molecules [19,20] PVA filament with higher peak intensity at this wavenumber suggested more asymmetric  $CH_2$  group present that formed complex structure in the matrix. PVA filament may be formulated to have rigid structure for 3DP application. With higher peak intensity at  $1710\text{ cm}^{-1}$  attributed for acetate group, the large amount of bulky acetate groups reduced flexibility of PVA that contributed to its rigid structure [16]. Acetate group with a hydrophobic property may be desired for PVA filament to resist moisture absorption and enhance its shelf life for commercial use [21].

Through this study, the molecular structure, and relative properties of PVA pellet and PVA filament were analyzed. This provided a better understanding of the material's properties for more relevant and appropriate applications. For example, the solubility of PVA was affected by its crystallinity whereby low crystallinity is associated with high water solubility [22]. PVA pellets with a relatively lower degree of crystallinity may be suitable for a bone scaffold that applies to wounds with a faster healing rate because it will dissolve within a relatively short time. PVA filament with higher rigidity may be applied to the load-bearing wound area.

### 3.2. Plasticizing effect of Poly(Vinyl) Alcohol variation

Plasticizer such as glycerol is commonly added to PVA to enhance its properties, especially the thermal properties. Plasticizers break the strong hydroxyl bond between the PVA molecules by forming chemical bonding with PVA. This will lower the melting and glass transition temperature of PVA to enhance its thermal processability [22]. Furthermore, the flexibility of PVA can be improved by increasing chain mobility [23]. This section analyzed the effect of glycerol added into the PVA pellet and PVA filament with the FTIR result.

Figure 2 and Figure 3 showed the FTIR curve of PVA pellet and filament respectively, for before and after plasticization with glycerol. By analyzing the graphs, glycerol was present in the plasticized PVA matrix with several additional peaks representing glycerol in the curve of plasticized PVA. These peaks included peak at a wavenumber of  $1038\text{ cm}^{-1}$  attributed for *OH* group,  $994\text{ cm}^{-1}$ , and  $669\text{ cm}^{-1}$ .

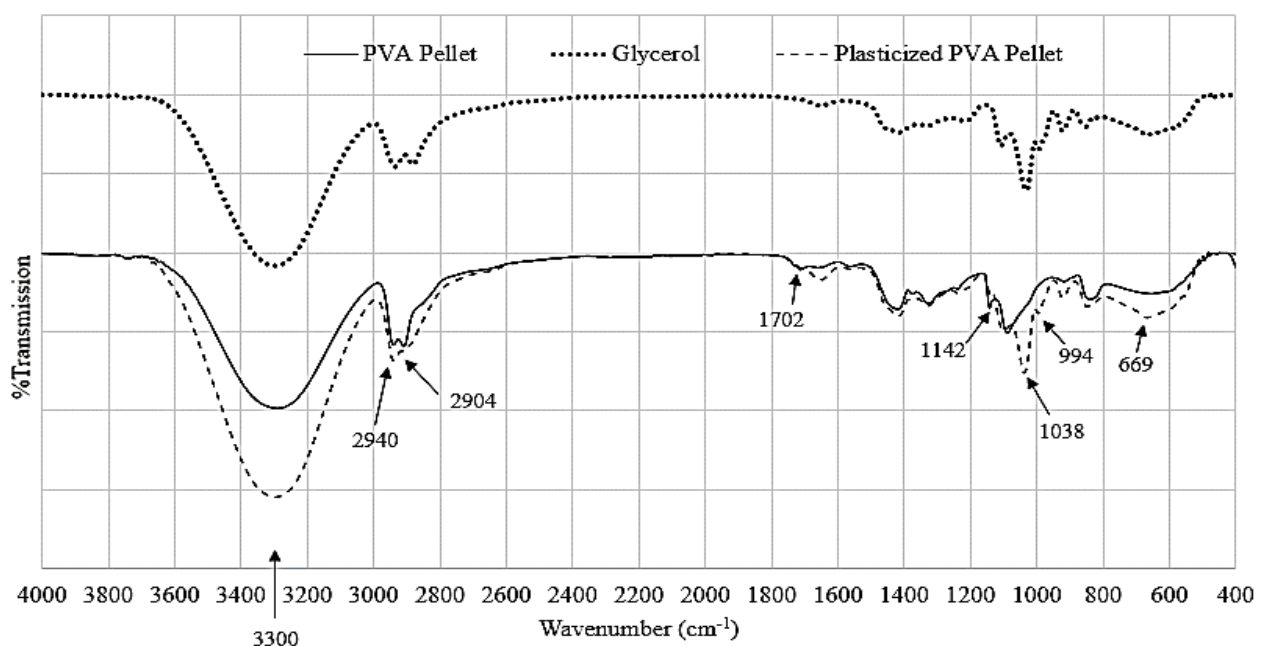


**Figure 2.** FTIR graph of PVA pellet before and after plasticized with glycerol

Interactions between glycerol and PVA were observed with the shifting of spectra. The shifting of largest hydroxyl band at  $3300\text{ cm}^{-1}$  indicated a good plasticizing effect as it weakened the hydrogen bonding between PVA molecules. This band with an increase in *OH* peak intensity may be due to the interaction and incorporation of glycerol. This result was supported by Sreekumar et. al [24] and Wang et. al [25] with increased *OH* peak intensity corresponding to lower water contact angle that suggested the blend was more hydrophilic. The shifting of *C = O* in acetate group from  $1702\text{ cm}^{-1}$  to  $1708\text{ cm}^{-1}$  indicated interaction occurred at this double bond that led to a decrease in the peak intensity. For this peak, the PVA pellet had a significant reduction in the intensity while PVA filament only had a slight reduction. This suggested PVA filament may have a saturated molecular structure with strong forces between neighboring molecules that caused difficulties in breaking this double bond.

There was no shifting observed at the duplet *CH*<sub>2</sub> group at near  $2904\text{ cm}^{-1}$  and  $2930\text{ cm}^{-1}$  for both PVA. However, the peak intensity of asymmetric *CH*<sub>2</sub> increased at higher wavenumber and symmetric *CH*<sub>2</sub> decreased at lower wavenumber. Interaction between PVA and glycerol may take place at symmetric *CH*<sub>2</sub> as it was easier to form bonds with low energy required to break the bonds. With this hypothesis, more complex structure represented by asymmetric *CH*<sub>2</sub> was formed.

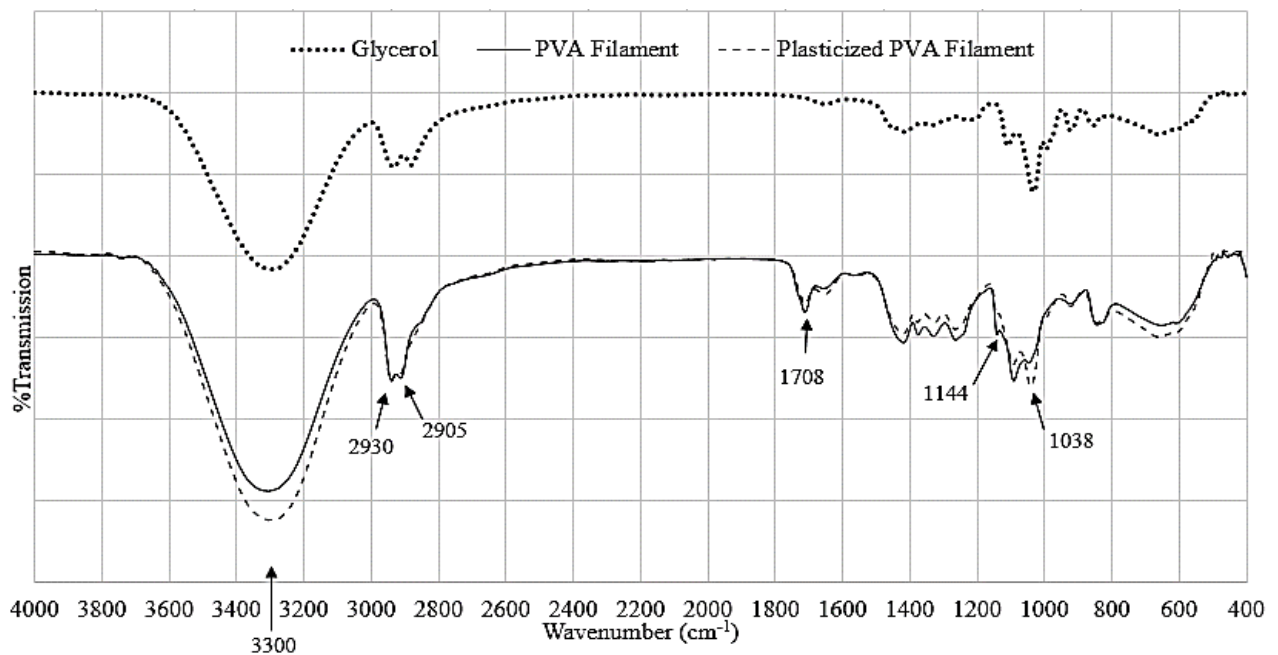


**Figure 3.** FTIR graph of PVA filament before and after plasticized with glycerol

Both PVA had different changes at the wavenumber of  $1142\text{ cm}^{-1}$  that gives information about crystallinity. In Fig. 2, the crystallinity of plasticized PVA pellet increased with an increase in peak intensity at  $1142\text{ cm}^{-1}$ . This result was supported by Boonsuk et. al [26] that reported the addition of glycerol increased crystallinity of PVA due to strong inter- and intramolecular hydrogen bonding between the components. However, the crystallinity of plasticized PVA filament decreased in Fig. 3. This may be due to the interaction between PVA filament and glycerol that increased the segmental mobility of PVA, which deteriorated the crystallinity region [21]. Aforementioned, the crystallinity is dependent on the hydrophilic/hydrophobic force balance [18]. The difference in changes of crystallinity for different PVA may be due to the difference in force balance within the molecular structure. This was further supported by PVA filament had more hydrophobic acetate group present in the PVA matrix as compared to the PVA pellet, which may cause the differences in the hydrophilic/hydrophobic force balance and crystallinity.

Although there were interactions between PVA and glycerol, the interactions were minimal with small shifting. The plasticizing effect was achieved but not effective. Therefore, crosslinking agents such as citric acid might be required to enhance the plasticizing effect for the optimum outcome of plasticization.

### 3.3. FTIR comparison for different bone scaffold fabrication method

A bone scaffold can be fabricated by two main categories, which are the conventional method and rapid prototyping with the composite of PVA and hydroxyapatite (HAp). Natural HAp derived from the fish bone of Spanish Mackerel (SM) was used. Scaffold fabricated by solution casting as a conventional method with the PVA pellet/HAp composite, and filament extrusion for Fused Deposition Modelling (FDM) as a rapid prototyping method with the PVA filament/HAp composite were studied and analyzed with FTIR in this section.

Figure 4 shows the FTIR graph for the solution casting of PVA pellet and HAp. The solution cast composite curve had overall increased in peak intensity as compared to the curve before solution casting. The increase in peak intensity primarily due to the incorporation of glycerol and HAp components in the PVA matrix. The FTIR curve of solution cast composite also showed further interaction between

glycerol and PVA, with evidence of the increased in peak intensity of duplet  $CH_2$  groups between  $2940\text{ cm}^{-1}$  and  $2899\text{ cm}^{-1}$ , absence of acetate group at  $1710\text{ cm}^{-1}$ , shifting of  $CO$  stretching peak between  $1089\text{ cm}^{-1}$  to  $1099\text{ cm}^{-1}$ , and the absence of  $CH_2$  bending at  $994\text{ cm}^{-1}$  on the solution cast curve. There was minimal interaction between PVA and HAp observed from the insignificant shifting of spectra. The spectra to justify this was the shifting of  $OH$  peak from  $3304\text{ cm}^{-1}$  to  $3292\text{ cm}^{-1}$ , and  $1039\text{ cm}^{-1}$  to  $1033\text{ cm}^{-1}$  due to the peak in HAp curve at  $1021\text{ cm}^{-1}$  from the HAp curve. Asran et. al [27] supported this finding with electrospun PVA/HAp composite showed interactions with FTIR result at this range of wavenumbers. The interaction occurred between HAp and PVA with the  $OH$  from PVA and HAp formed bonds with  $Ca^{2+}$  from HAp [17]. The overall crystallinity of the solution cast curve increased with peak increment and shifting at  $1140\text{ cm}^{-1}$ . The interaction between PVA and HAp had modified the crystallinity of the composite.

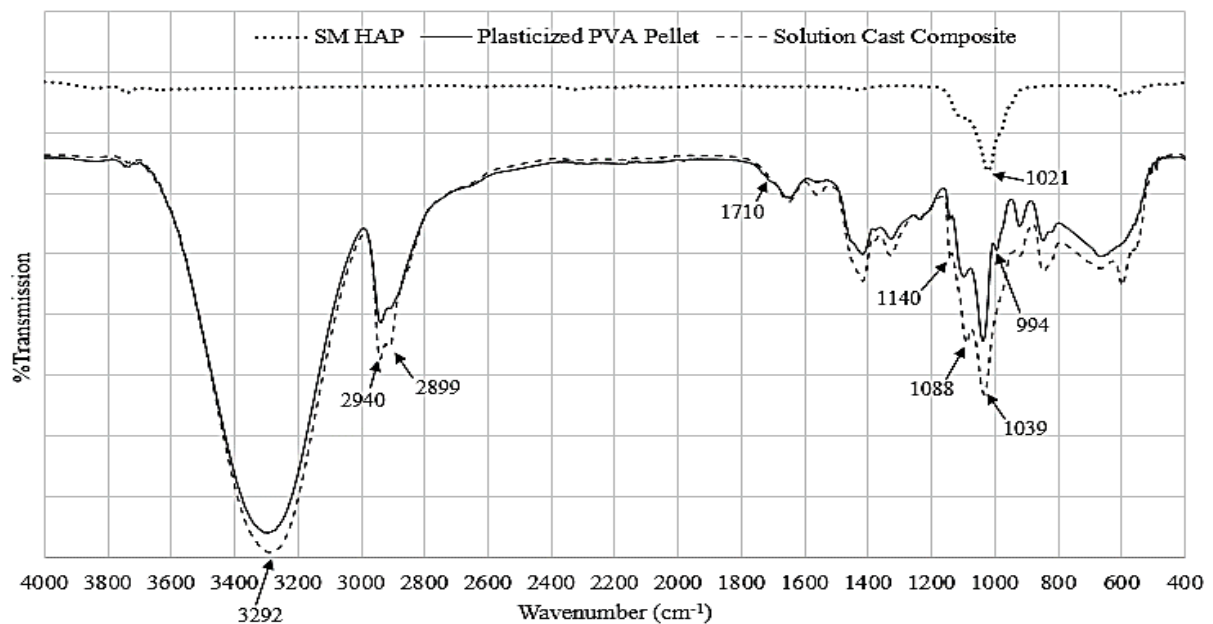


**Figure 4.** FTIR graph of PVA pellet and HAp composite before and after solution casting

Figure 5 shows the FTIR graph of the extruded composite of PVA filament and HAp. The extruded curve showed an overall decrease in peak intensity as compared to the curve before extrusion. The hot-melt extrusion process caused evaporation of volatile component, especially water that led to decreased at the large characteristic  $OH$  band at  $3300\text{ cm}^{-1}$  [28]. Decreased in  $OH$  peak intensity also indicated possible formation of amorphous structure with PVA chain started to unfold due to thermal heating [29]. There were no peaks shifting observed with the exception at the duplet of  $CH_2$  near  $2800\text{ cm}^{-1}$  to  $3000\text{ cm}^{-1}$ . Li et. al [30] reported a similar result. This suggested minimal or no interaction occurred between HAp and PVA filament at those functional groups during the hot-melt extrusion process. This may due to the saturated and complex molecular structure of PVA filament that makes it difficult for HAp to break the bonds for interaction to occur. The  $CH_2$  duplet group had drastic shifting and increased in peak intensity. These duplet groups responded to temperature induced changes whereby high temperature will cause an increase in the peak intensity, as reported by Garidel et. al [31]. Moreover, asymmetric  $CH_2$  at  $2915\text{ cm}^{-1}$  with higher vibrational energy can absorb more thermal energy from the extrusion process. More saturated asymmetric  $CH_2$  group present suggested complex molecular structure in extruded PVA filament. The shifting of duplet group indicated interaction occurred at this functional group because the single bond of  $CH_2$  may be easier to break by the HAp and/or glycerol. On top of that, the PVA molecules were stretched and aligned as it reached its melting point during the hot-melt extrusion process [32]. With the shear forces from extrusion, this enhanced the interaction of PVA

with other component, especially glycerol. The thermally induced physical crosslinking between PVA and glycerol may cause random chain rearrangement and destroyed the crystallinity of polymer [29]. This was supported by the reduction in peak intensity at  $1140\text{ cm}^{-1}$ . Moreover, addition of amorphous HAP may decreased the crystallinity of PVA as well [33].

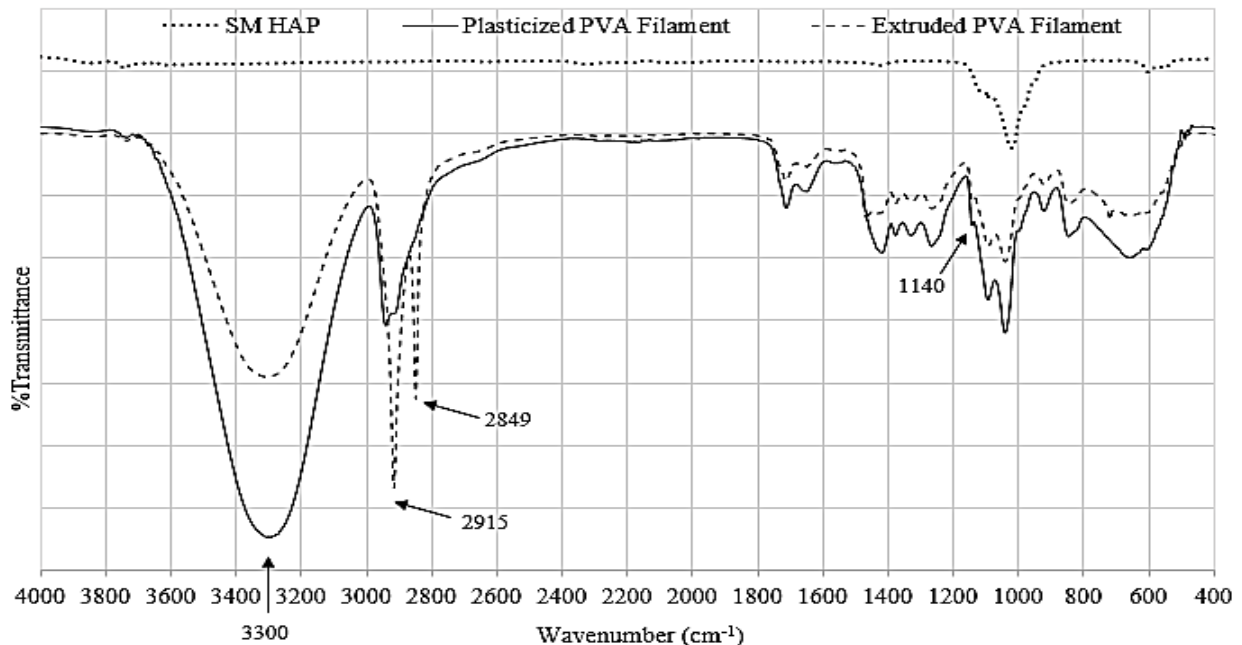


**Figure 5.** FTIR graph of PVA filament and HAp composite before and after filament extrusion

The effect of different fabrication methods on the molecular structure of composite had been studied. In summary, the solution casting method incorporated glycerol and HAP into the PVA matrix. The crystallinity also increased through the solution casting method. The hot-melt extrusion method losses the volatile groups during the high temperature operations and reduced the crystallinity of the composite. In terms of the interaction between PVA and HAp, although minimal interactions were observed, the solution casting method showed relatively significant interaction as compared to the extruded method. The high agglomeration rate of HAP and high viscosity of the polymer solution may hinder and minimized interactions of the composite [34]. Additional components or processes might be required to enhance the interaction between HAp and PVA for optimum bone scaffold properties especially in terms of osteoconductive and mechanical properties.

### 3.4. Differences in hydroxyapatite derived from different fish bones

Plasticizer Natural hydroxyapatite (HAp) can be derived from fish bones. The fish bones used for this study were the Spanish Mackerel (SM) and Whitefin Wolf Herring (WWH). These fishes known to be “ikan tenggiri” and “ikan parang” by the locals are common fishes that can be found in Malaysia. This section interested to study vibrational spectroscopy of natural HAp derived from different fish bones and their properties.

Figure 6 shows the FTIR of SM and WWH HAp. The FTIR curve of these naturally derived HAp had good agreement with FTIR reported for synthetic HAp [34, 35] and naturally derived HAp [37]. Both curves had similar peaks but WWH had overall higher peak intensities than SM. The crystallinity of HAp was observed from the FTIR graph with WWH had higher crystallinity than SM. The first evidence was the antisymmetric mode of  $PO_4^{3-}$  group at spectral region between  $1040\text{ cm}^{-1}$  and  $1090\text{ cm}^{-1}$ . As

proposed by Pleshko et. al [38] and further validated by Poralan et. al [37], the peaks within this range of wavenumber give information about the crystallinity of HAp. The smaller the area of this phosphate-substitution side, the higher the degree of crystallinity of the HAp. WWH had a smaller area than SM at this side suggested WWH had higher crystallinity. The second evidence was the bending of  $PO_4^{3-}$  at  $500\text{ cm}^{-1}$  to  $630\text{ cm}^{-1}$ . Sharp duplet peaks at this range of wavenumber indicates high crystallinity as proposed by Poralan et. al [37]. WWH with higher peak intensity of the duplet peak as compared to SM indicated WWH had higher crystallinity. On the other hand,  $\beta$  type tri-calcium phosphate ( $\beta - TCP$ ) may be present in the natural HAp with a peak around  $960\text{ cm}^{-1}$  and this finding correlate to other naturally derived HAp [7,39]. The small peak at  $1420\text{ cm}^{-1}$  on SM and  $1425\text{ cm}^{-1}$  on WWH curve attributed to  $CO_3^{2-}$  carbonate ions that associated to amorphous phase of HAp [40]. It present as impurities and found in traces amount by the other authors [37,41]. The small peak may due to decomposition of carbonate ions into carbon dioxide during the high temperature calcination process [7]. Hydroxyl groups also present with small peaks at  $3600\text{ cm}^{-1}$  to  $3736\text{ cm}^{-1}$  for both SM and WWH. WWH had more hydroxyl groups with the extra peak at  $631\text{ cm}^{-1}$  that was absent in SM curve. This result correlate to findings by Boutinguiza et. al [39] that propose biological HAp has nonstoichiometric composition with less hydroxyl content.

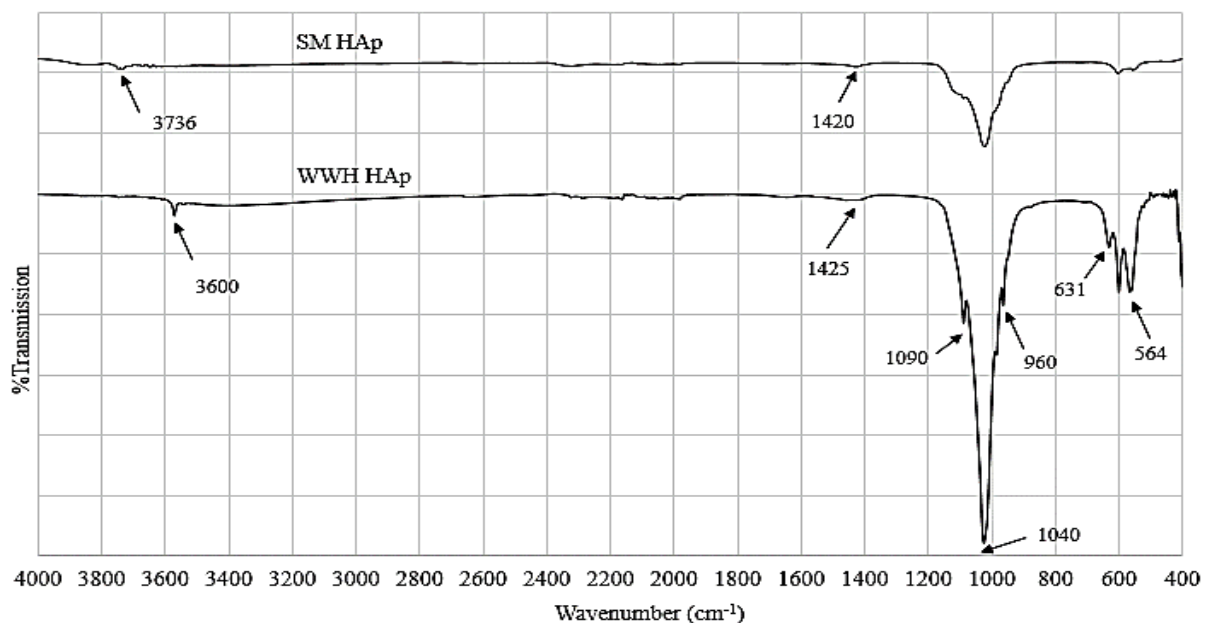


**Figure 6.** FTIR graph of hydroxyapatite derived from fish bone of SM and WWH

The EDX result in Table 2 showed WWH had calcium to phosphorus (Ca/P) ratio of 1.92 and SM with 1.77. Both HAp had a non-stoichiometric ratio due to the presence of metal ions that promotes bone reconstruction [42]. SM had a ratio closer to the stoichiometric ratio of 1.67 while WWH had a higher ratio than the stoichiometric ratio. This suggested SM had the characteristic of a stoichiometric ratio with maximum strength and structural rigidity that closed to natural stoichiometric apatite in human bone [43]. The higher Ca/P ratio for both SM and WWH indicated the presence of B-type carbonate phosphate, a mineral similar to human bones that promotes cell adhesion [39]. WWH had more of this apatite with a higher Ca/P ratio and further supported by the higher carbonate ions peak at  $1420\text{ cm}^{-1}$  from FTIR curve of WWH HAp.

**Table 2.** Calcium to phosphorus ratio of natural HAp derived from different fish bones

Sources of HAp for 30HAp/PVA	Ca/P Ratio (wt%)
Spanish Mackerel (SM)	1.77
Whitefin Wolf Herring (WWH)	1.92
Stoichiometry	1.67

In summary, both HAp contained a small amount of  $\beta$  - TCP that promotes osteoconduction [7,39]. From the FTIR result, WWH had higher crystallinity than SM. Crystallinity has an inverse relationship with solubility that affects bone consistency and osteoconductivity. HAp with similar crystallinity as human bone can easily interact with the body systems with a lower risk of a rejection response. Therefore, SM with a relatively lower crystallinity can be applied to wounds with shorter healing time with its higher solubility. The higher crystallinity WWH may be suitable for bone scaffold applied on wounds that required longer healing time due to its low solubility. From EDX result, SM with stronger structure can be applied to loading-bearing area that experiences higher stress whereas WWH can be useful in the application that priorities rapid wound healing.

### 3.5. Fishbones hydroxyapatite with poly(vinyl) alcohol composites

This section discussed the characterization of bone scaffold fabricated by solution casting method with PVA pellet and HAp. The HAp was varied by variation in HAp (SM and WWH) and its loading (0, 2.5, 5, 10, 20, and 30%).

The effect of HAp added into PVA was discussed in the earlier section. The FTIR in Fig. 7 discussed the effect of different loading of SM HAp. The crystallinity of composite was affected by the loading of HAp as shown in peak wavenumber of  $1140\text{ cm}^{-1}$ . This peak intensity increased at low HAp loading but started to reduce with HAp loading from 10% onwards. This suggested the HAp interacted with PVA improved the crystallinity at low loading. However, at high loading, the dominating brittle property of HAp and agglomeration may disrupt the crystallinity [29,34]. The peak at the wavenumber of  $1033\text{ cm}^{-1}$  attributed to OH group for PVA and  $PO_4^{3-}$  for HAp, showed interesting changes as well. The peak shifted upon addition of HAp at 2.5% loading and does not further shift despite increasing loading of HAp. The initial addition of HAp induced interactions but loading of HAp does not affect the interaction. The initial shifting of this peak suggested interaction may occur between HAp and PVA. This occurrence of interaction indicated HAp was uniformly dispersed in PVA matrix that enabled the formation of the chemical bond between these components [17]. The gradual increase in this peak intensity at  $1033\text{ cm}^{-1}$  as HAp concentration increased due to the increase in phosphate group in the matrix. The notable increased in new peak intensity at  $596\text{ cm}^{-1}$  attributed to  $PO_4^{3-}$  also supported this finding. Several peaks experienced no change in peak intensities despite loading of HAp, such as the OH band at  $3300\text{ cm}^{-1}$ , the duplet  $CH_2$  group between  $2940\text{ cm}^{-1}$  and  $2899\text{ cm}^{-1}$ ,  $1650\text{ cm}^{-1}$  attributed to OH from water, etc.

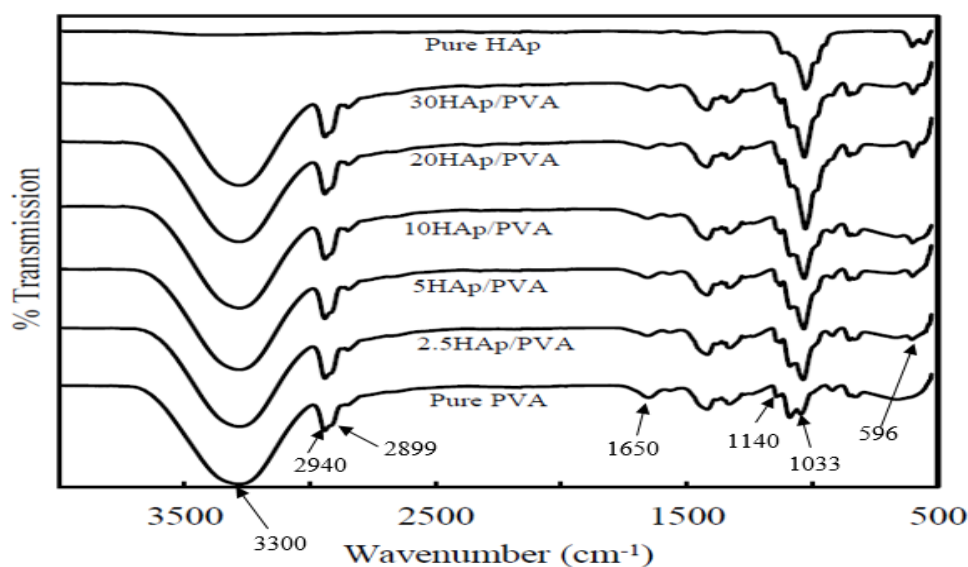


**Figure 7.** FTIR graph of film with composite of PVA and different loading of HAp derived from fish bone of SM

The TGA result in Fig. 8 showed three stages of weight loss from 30 °C to 275 °C, 275 °C to 320 °C, and 320 °C to 520 °C. The first weight loss was due to the evaporation of volatile composite, primarily water. The second weight loss was the degradation of the side chain and *OH* group of PVA. The third weight loss was due to the degradation of the main chain of PVA with a carbonation reaction. There was no specific trend in the first two stages of weight loss with increased loading of HAp. This may be due to PVA being the dominating component affecting the TGA curves at this range of temperatures. However, after 500 °C when all PVA was decomposed, a clear trend was observed whereby higher loading of HAp had lower weight loss. At high temperatures, all organic components would be burned off and left with the high thermal stability HAp. Higher loading of HAp had lower weight loss due to the higher concentration of remaining metal ions present in its composition, as compared to the lower loading of HAp.

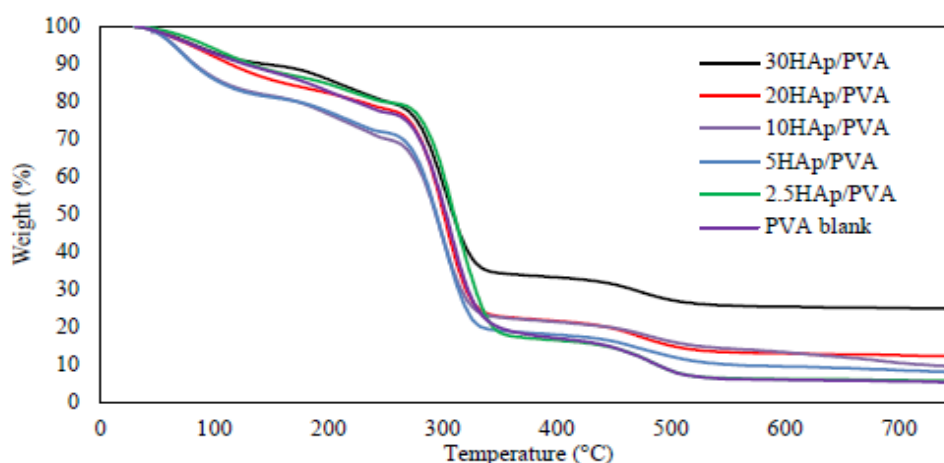


**Figure 8.** TGA curve of film with composite of PVA and different loading of HAp derived from fish bone of SM

The SEM imaging was done at the fracture site of PVA/HAp composite at 2.5% and 30% loading. Figure 9 (a) showed the fracture site at 2.5% loading of SM HAp composite with a clean fracture pattern. This may be due to the low concentration of HAp that homogeneously dispersed in the PVA matrix or poor bonding between HAp and PVA, which caused only PVA contributing to the fracture pattern [44]. Figure 9 (b) of 2.5% WWH composite showed a rough and pulled pattern. The pulled pattern suggested this composite had a better plasticizing effect and good elasticity. The rough surface may be due to the high surface energy of WWH that caused the soft agglomeration of HAp at low loading [45]. The agglomeration that acts as stress concentration points caused poor mechanical properties of the composite. Comparing Fig. 10 for 30% high loading of (a) SM and (b) WWH composite, SEM showed a saturated matrix whereby WWH had more agglomeration cluster as compared to SM at the same magnification. This further verified WWH had higher surface energy that tends to cause HAp agglomeration in the composite.

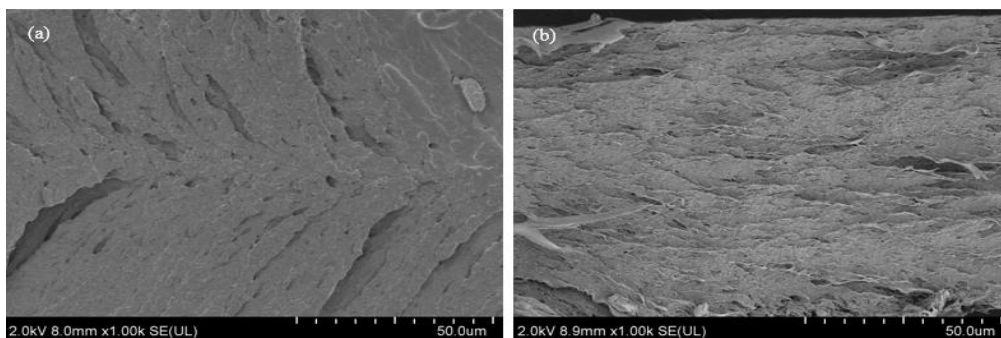


**Figure 9.** SEM of fractured composite of PVA and 2.5% HAp loading from fish bones of (a) SM and (b) WWH

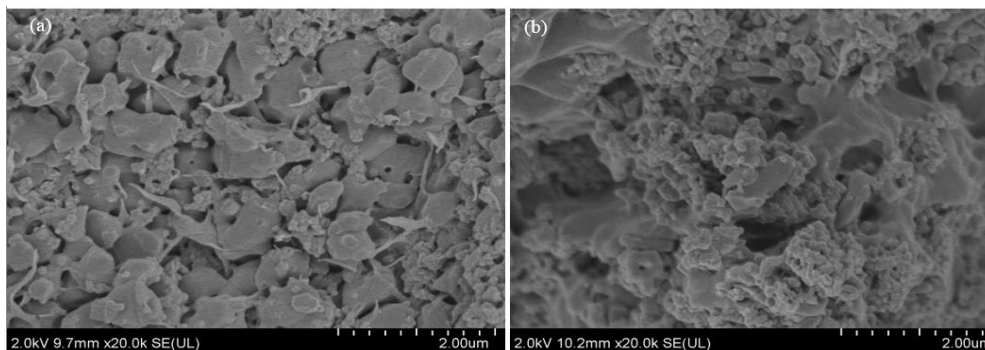


**Figure 10.** SEM of fractured composite of PVA and 30.0% HAp loading from fish bones of (a) SM and (b) WWH

The mechanical properties of PVA/HAp composite were analyzed in terms of tensile strength with Fig. 11 (a) and elongation at break with Fig. 11 (b). The addition of HAp into the PVA matrix improved the tensile strength due to interactions that formed strong hydrogen bond and/or hydroxyl-calcium-hydroxyl bonds that improved the mechanical performance of composite [17]. The load applied was deflected by the interfacial bonding that further reinforced the toughness of structure [41]. The elongation of break was decreased upon the addition of HAp due to the presence of brittle HAp that reduced the elasticity of composite. As the loading of HAp increased, both mechanical properties decreased. Other than the increase in the concentration of brittle HAp, agglomeration of HAp may cause deterioration of the mechanical properties. The agglomeration blocked the dislocation motion when molecules slipped against each other to deflect the load applied. This formed stress concentrated locations where mechanical failure starts to occur. In Fig. 11 (a), WWH had overall lower tensile strength as compared to SM. This is due to the high crystallinity of WWH with brittle properties and higher surface energy that tend to agglomerate HAp [46]. From Fig. 11 (b), WWH had higher elongation at break as compared

to SM that suggested WWH composite had better interactions and plasticizing effect. This was further supported by relatively more hydroxyl groups observed in FTIR of WWH that could form more interactions between HAp with PVA and glycerol. As compared to the gradually decreasing trend in Fig. 11 (b), WWH HAp had drastically decreased at 30% loading. This might due to the relatively higher surface area of WWH that formed more agglomeration and drastically affected the mechanical property of WWH composite. SEM imaging also supported this hypothesis with more agglomerations formed in 30% WWH HAp. ANOVA 2-way statistical analysis was performed to determine if mechanical properties of the composite were affected by HAp loading and variations. With a threshold value of 0.05, both factors contributed to tensile strength and elongation at break, with variation in HAp as the dominant factor. Therefore, it is crucial to select suitable HAp with properties that tailored to different applications of the bone scaffold.

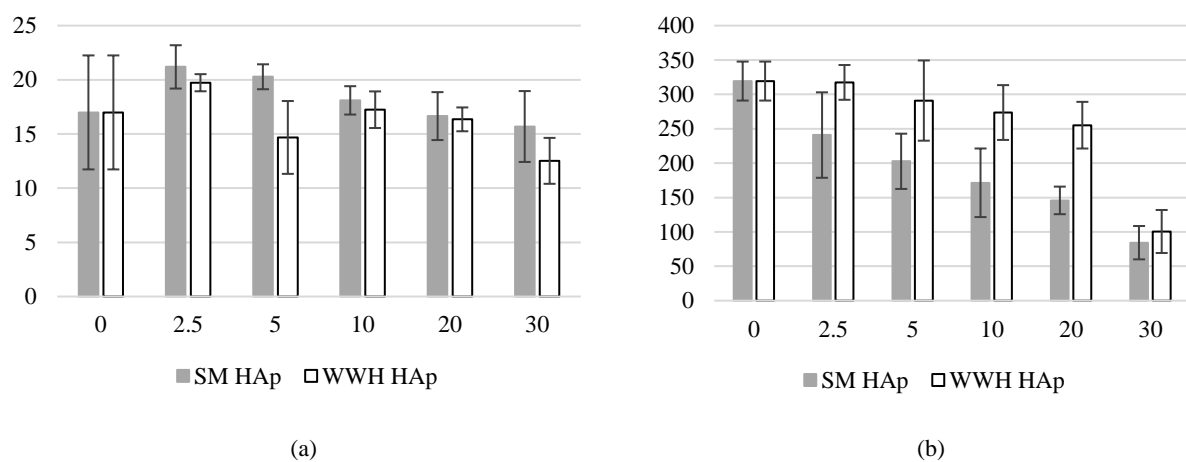


**Figure 11.** Mechanical properties of different variations and loading of HAp in PVA/HAp composite with (a) tensile strength and (b) elongation at break

#### 4. Conclusions

FTIR spectroscopy has proven to be a useful tool to characterize the molecular structure, interactions, and relevant properties. In terms of variations in PVA in the form of pellet and filament, the analysis showed PVA filament had complex saturated molecular structure, relatively higher crystallinity, rigid, and more hydrophobic nature than PVA pellet. Minimal interactions between PVA and glycerol were observed with the slight shifting of spectra and changes in peak intensity. This suggested crosslinking agent may be required to enhance the plasticizing effect. PVA pellet showed slightly more evidence of interaction with glycerol, as compared to PVA filament with saturated molecular structure. The plasticizing effect of the PVA pellet increased the crystallinity of composite while PVA filament showed decrement. The different responses reflected on crystallinity may arise from the difference in hydrophilic and hydrophobic force balance present in the PVA variations. Similar findings were observed for the variation of the scaffold fabrication method. The FTIR of solution casting film indicates incorporation of components into the matrix and increased in crystallinity, while the extruded filament showed evaporation of volatile components with the hot-melt extrusion process with decreased crystallinity. Minimal interactions were observed for both methods, but solution casting illustrated slightly more interaction between PVA and HAp composite as compared to extrusion. The FTIR analysis of natural HAp derived from fish bone of Spanish Mackerel (SM) and Whitefin Wolf Herring (WWH) showed WWH had higher crystallinity than SM. Both HAp contains a small amount of  $\beta$  type tri-calcium phosphate ( $\beta$  - TCP) that possessed good biodegradability and cell compatibility. SM had calcium to phosphate (Ca/P) ratio closer to the stoichiometry ratio that indicates SM had optimum mechanical strength corresponding to human bone. WWH had a higher Ca/P ratio than stoichiometric suggested the

presence of B-type carbonate phosphate that promotes cell adhesion. The loading of HAp does not affect the interactions of composite from the FTIR graph and the thermal properties from the TGA curves. However, it did affect the crystallinity of composite that increased at low HAp loading and further decreased at HAp loading of 10% onwards. This is due to the agglomeration of HAp at higher loading that formed stress points where fracture begins, as supported by SEM. Upon the addition of HAp into PVA, the tensile strength of composite increased due to strong bonds formed from the interaction of PVA and HAp, while elongation at break decreased due to a reduction in elasticity by the brittle HAp. As the loading of HAp increased, both mechanical properties decreased due to an increase in the concentration of brittle HAp and agglomeration. WWH composite portrays lower tensile strength due to its higher crystallinity with brittle properties and higher surface energy that prone to agglomeration. WWH also had higher elongation at break due to better plasticizing effect, evidenced by more hydroxyl groups observed from FTIR and pulled fracture pattern in SEM. ANOVA analysis confirmed HAp loading and variations contributed to changes in mechanical properties, with HAp variation being the most influential factor.

The material's properties and interactions were studied with FTIR spectroscopy analysis to provide information for its application. Crystallinity had an inverse relationship with solubility which is a crucial parameter of the bone scaffold. The composition and mechanical properties greatly affect the performance and application of bone scaffolds. With the same objective, future work can be performed to provide further justification for this work such as XRD to justify crystallinity, DSC to justify thermal properties, BET to evaluate the pore structure, swelling test to study the solubility, and more. This work can be expanded to study the effect of these materials' interaction on scaffold properties fabricated by other scaffold fabrication methods. These works can be performed as an effort of realizing the feasibility of PVA and naturally derived HAp from fish bones for the application of bone tissue engineering.

## 5. Acknowledgments

The authors are grateful for the financial support from Taylor's Internal Research Grant Scheme – Major Funding scheme (TiRGS-MFS) with code of TRGS/MFS/1/2018/SOE/002 to complete this study.

## 6. References

- [1] Kalfas I H 2001 Principles of bone healing *Neurosurg. Focus* **10** 1–4
- [2] Howard D, Buttery L D, Shakesheff K M and Roberts S J 2008 Tissue engineering: strategies, stem cells and scaffolds *J. Anat.* **213** 66
- [3] Eltom A, Zhong G and Muhammad A 2019 Scaffold techniques and designs in tissue engineering functions and purposes: A review *Adv. Mater. Sci. Eng.* **2019** 1–13
- [4] Ghassemi T, Shahroodi A, Ebrahimzadeh M H, Mousavian A, Movaffagh J and Moradi A 2018 Current concepts in scaffolding for bone tissue engineering *Arch. bone Jt. Surg.* **6** 90–9
- [5] Wu J, Chen N, Bai F and Wang Q 2018 Preparation of poly(vinyl alcohol)/poly(lactic acid)/hydroxyapatite bioactive nanocomposites for fused deposition modeling *Polym. Compos.* **39** E508–18
- [6] Mohd Pu'ad N A S, Koshy P, Abdullah H Z, Idris M I and Lee T C 2019 Syntheses of hydroxyapatite from natural sources *Heliyon* **5** e01588
- [7] Zairin D A and Phang S W 2018 Temperature Effect on Natural Hydroxyapatite Obtained from Fish Bones for Bone Tissue Engineering *J. Eng. Sci. Technol.* 39–51
- [8] Wiria F E, Chua C K, Leong K F, Quah Z Y, Chandrasekaran M and Lee M W 2008 Improved biocomposite development of poly(vinyl alcohol) and hydroxyapatite for tissue engineering scaffold fabrication using selective laser sintering *J. Mater. Sci. Mater. Med.* **19** 989–96
- [9] Chen N, Li L and Wang Q 2007 New technology for thermal processing of poly(vinyl alcohol) *Plast. Rubber Compos.* **36** 283–90
- [10] Zhou X Y, Cui Y F, Jia D M and Xie D 2009 Effect of a complex plasticizer on the structure and properties of the thermoplastic PVA/starch blends *Polym. - Plast. Technol. Eng.* **48** 489–95

- [11] Pandey G C, Kumar A and Garg R K 2001 A novel approach for the determination of physicomechanical properties of polymers by vibrational spectroscopy: The tensile strength of polybutadiene rubber *J. Appl. Polym. Sci.* **82** 2135–9
- [12] Gunasekaran S, Natarajan R K and Kala A 2007 FTIR spectra and mechanical strength analysis of some selected rubber derivatives *Spectrochim. Acta - Part A Mol. Biomol. Spectrosc.* **68** 323–30
- [13] Cox S C, Thornby J A, Gibbons G J, Williams M A and Mallick K K 2015 3D printing of porous hydroxyapatite scaffolds intended for use in bone tissue engineering applications *Mater. Sci. Eng. C* **47** 237–47
- [14] Krimm S, Liang C Y and Sutherland G B B . 1956 Infrared spectra of high polymers. V. Polyvinyl alcohol *J. Polym. Sci.* **XXII** 227–47
- [15] Awada H and Daneault C 2015 Chemical modification of poly(vinyl alcohol) in water *Appl. Sci.* **5** 840–50
- [16] Mansur H S, Sadahira C M, Souza A N and Mansur A A P 2008 FTIR spectroscopy characterization of poly (vinyl alcohol) hydrogel with different hydrolysis degree and chemically crosslinked with glutaraldehyde *Mater. Sci. Eng. C* **28** 539–48
- [17] Fenglan X, Yubao L, Xuejiang W, Jie W and Aiping Y 2004 Preparation and characterization of nano-hydroxyapatite/poly(vinyl alcohol) hydrogel biocomposite *J. Mater. Sci.* **39** 5669–72
- [18] Mansur H S, Oréface R L and Mansur A A P 2004 Characterization of poly(vinyl alcohol)/poly(ethylene glycol) hydrogels and PVA-derived hybrids by small-angle X-ray scattering and FTIR spectroscopy *Polymer (Guildf)*. **45** 7193–202
- [19] Kozai T, Yamashita S, Hirochi K, Miyagawa H, Tsurumachi N, Koshiha S, Nakanishi S and Itoh H 2012 Molecular vibrational dynamics in polyvinyl alcohol studied by femtosecond coherent Anti-Stokes Raman spectroscopy *Chem. Phys. Lett.* **553** 26–9
- [20] Abdal-hay A, In C and Kyoo J 2014 An in situ hydrothermal fabrication process of poly (vinyl alcohol) / apatite-like nanocomposites with improved thermal and mechanical properties *Ceram. Int.* **40** 4995–5000
- [21] Jang J and Lee D K 2003 Plasticizer effect on the melting and crystallization behavior of polyvinyl alcohol *Polymer (Guildf)*. **44** 8139–46
- [22] Fink J K 2020 *The Chemistry of Bio-Based Polymers* (John Wiley & Sons)
- [23] Fong R J, Robertson A, Mallon P E and Thompson R L 2018 The impact of plasticizer and degree of hydrolysis on free volume of poly(vinyl alcohol) films *Polymers (Basel)*. **10** 1036
- [24] Sreekumar P A and Al-harhi M A 2012 Effect of glycerol on thermal and mechanical properties of polyvinyl alcohol/starch blends *J. Appl. Polym. Sci.* **123** 135–42
- [25] Wang S, Ren J and Kong W 2014 Influence of urea and glycerol on functional properties of biodegradable PVA / xylan composite films *Cellulose* **21** 495–505
- [26] Boonsuk P, Kaewtatip K, Chantarak S, Kelarakis A and Chaibundit C 2018 Super-tough biodegradable poly (vinyl alcohol) / poly (vinyl pyrrolidone ) blends plasticized by glycerol and sorbitol *J. Appl. Polym. Sci.* **125** 1–8
- [27] Asran A S, Henning S and Michler G H 2010 Polyvinyl alcohol-collagen-hydroxyapatite biocomposite nanofibrous scaffold: Mimicking the key features of natural bone at the nanoscale level *Polymer (Guildf)*. **51** 868–76
- [28] Hossain U H, Seidl T and Ensinger W 2014 Combined in situ infrared and mass spectrometric analysis of high-energy heavy ion induced degradation of polyvinyl polymers *Polym. Chem.* **5** 1001–12
- [29] Mohsin M, Hossin A and Haik Y 2011 Thermal and mechanical properties of poly(vinyl alcohol) plasticized with glycerol *J. Appl. Polym. Sci.* **122** 3102–9
- [30] Li Z, de Souza L R, Litina C, Markaki A E and Al-Tabbaa A 2019 Feasibility of using 3D printed polyvinyl alcohol *Materials (Basel)*. **12** 1–13
- [31] Garidel P, Blume A and Hübner W 2000 A fourier transform infrared spectroscopic study of the interaction of alkaline earth cations with the negatively charged phospholipid 1,2-dimyristoyl-sn-glycero-3-phosphoglycerol *Biochim. Biophys. Acta - Biomembr.* **1466** 245–59
- [32] Follain N, Joly C, Dole P and Bliard C 2005 Properties of starch based blends. Part 2. Influence

- of poly vinyl alcohol addition and photocrosslinking on starch based materials mechanical properties *Carbohydr. Polym.* **60** 185–92
- [33] Yang C C, Li Y J, Chiu S J, Lee K T, Chien W C and Huang C A 2008 A direct borohydride fuel cell based on poly(vinyl alcohol)/hydroxyapatite composite polymer electrolyte membrane *J. Power Sources* **184** 95–8
- [34] Chua C K, Leong K F, Tan K H, Wiria F E and Cheah C M 2004 Development of tissue scaffolds using selective laser sintering of polyvinyl alcohol/hydroxyapatite biocomposite for craniofacial and joint defects *J. Mater. Sci. Mater. Med.* **15** 1113–21
- [35] Naga S M, El-Maghraby H F, Mahmoud E M, Talaat M S and Ibrhim A M 2015 Preparation and characterization of highly porous ceramic scaffolds based on thermally treated fish bone *Ceram. Int.* **41** 15010–6
- [36] Kebiroglu M H, Orek C, Bulut N, Kaygili O, Keser S and Ates T 2017 Temperature dependent structural and vibrational properties of hydroxyapatite: A theoretical and experimental study *Ceram. Int.* **43** 15899–904
- [37] Poralan G M, Gambe J E, Alcantara E M and Vequizo R . 2015 X-ray diffraction and infrared spectroscopy analyses on the crystallinity of engineered biological hydroxyapatite for medical application *Applied Physics and Materials Science* vol 79 (IOP Publishing)
- [38] Pleshko N, Boskey A and Mendelsohn R 1991 Novel infrared spectroscopic method for the determination of crystallinity of hydroxyapatite minerals *Biophys. J.* **60** 786–93
- [39] Boutinguiza M, Pou J, Comesaña R, Lusquiños F, De Carlos A and León B 2012 Biological hydroxyapatite obtained from fish bones *Mater. Sci. Eng. C* **32** 478–86
- [40] Xu G, Aksay I A and Groves J T 2001 Continuous crystalline carbonate apatite thin films: A biomimetic approach *J. Am. Chem. Soc.* **123** 2196–203
- [41] Wei Q, Wang Y, Li X, Wang K, Chai W and Zhang Y 2015 Study the bonding mechanism of binders on hydroxyapatite surface and mechanical properties for 3DP fabrication bone *J. Mech. Behav. Biomed. Mater.* **57**
- [42] Akram M, Ahmed R, Shakir I, Ibrahim W A W and Hussain R 2014 Extracting hydroxyapatite and its precursors from natural resources *J. Mater. Sci.* **49** 1461–75
- [43] Lett J A, Sundareswari M, Ravichandran K and Sagadevan S 2018 The fabrication of porous hydroxyapatite scaffold using gaur gum as a natural binder *Dig. J. Nanomater. Biostructures* **13** 235–43
- [44] Thanomsilp C, Cauchi-Savona S, Peijs T and Posyachinda S 2007 Use of rice husk powder as a substitute for CaCO<sub>3</sub> in thermoset-based molding compounds *J. Biobased Mater. Bioenergy* **1** 87–93
- [45] Bardhan R, Mahata S and Mondal B 2011 Processing of natural resourced hydroxyapatite from eggshell waste by wet precipitation method *Adv. Appl. Ceram.* **110** 80–6
- [46] Haghshenas M 2017 Mechanical characteristics of biodegradable magnesium matrix composites: A review *J. Magnes. Alloy.* **5** 189–201